RSC Advances

PAPER

Cite this: *RSC Adv.*, 2020, **10**, 5988

The effects of different factors on the removal mechanism of Pb(II) by biochar-supported carbon nanotube composites

Yuewei Yang,†* Fengfei Sun,† Jing Li, Junfeng Chen and Meizhen Tang

Received 13th November 2019
Accepted 13th January 2020

DOI: 10.1039/c9ra09470a

rsc.li/rsc-advances

Herein, biochar-supported nanomaterials were synthesized using a mixture of chestnut shells and carbon nanotubes *via* slow pyrolysis at 600 °C for 1 h. Then, the adsorption ability of chestnut shell-carbon nanotubes (CS-CNTs) towards the removal of aqueous Pb(II) was tested. The removal capacity of Pb(II) by CS-CNT was 1641 mg g^{-1}, which was significantly higher than that by the biochar of chestnut shells (CSs) (1568 mg g^{-1}), which demonstrated that the sorption capacity could be improved by the carbon nanotubes. The factors studied here indicated that the adsorption was rapid in the initial 15 min under the conditions of the Pb(II) concentration of 50 mg L^{-1} and the pH value of 5, and the values reached 1417 mg g^{-1} and 1584 mg g^{-1}. The adsorption rate and capacity increased on increasing the concentration of NaCl. The sorption reaction was consistent with the Langmuir model, indicating a mono-layer adsorption behavior. The adsorption process can also be defined *via* the pseudo-second-order model, suggesting that the adsorption of Pb(II) might be controlled by chemisorption. After carrying out four cycles of adsorption–desorption experiments, the adsorption rates of CS and CS-CNT remained at 82.92% and 88.91%, respectively, indicating that the biochar samples had stable and excellent sorption ability for heavy metals and huge application value. Thus, this study would provide a promising sorbent for the treatment and remediation of metal contaminants.

1. Introduction

With the rapid development of modern industries and agriculture, the presence of lead (Pb) in the aquatic environment has become a major concern for researchers worldwide. Because of their toxicity, persistence and non-degradation, heavy metals tend to accumulate in living organisms; this poses a serious threat to the living organisms and human health and gradually affects the entire ecosystem.[1,2] The removal of Pb(II) from wastewater has become an urgent problem in environmental protection. Therefore, the development of scientific and effective methods to deal with the wastewater polluted by Pb(II) has become a research hotspot.

Several methods, such as advanced oxidation, biological treatment, electrochemical technologies, and adsorption, have been widely used to remove heavy metals from wastewater.[3–6] The adsorption technology is a preferred approach because of its safety, efficiency, and economic feasibility; moreover, it can be performed using low-cost sorbents in the adsorption process.[7] Biochar is the most popular sorbent in the sorption process, and many studies have been carried out on biochar. Biochar, which can be produced by the oxygen-restricted pyrolysis of biological organic materials[8,9] and has numerous environmental benefits and wide application potential, has attracted considerable attention from many researchers.[10] It is not only a stable porous carbon material but also a low-cost sorbent with a high specific surface area and abundant surface functional groups; due to these properties, biochar is widely applied for increasing soil fertility and adsorption performance to alleviate environmental pollution and reduce environmental risks.[11–15] As an economical, green and efficient sorbent, biochar has been widely used in the study of heavy metal adsorption.[16] However, it has been found that biochar easily causes secondary pollution during the adsorption of heavy metals.[17,18] With the further development of biochar, the preparation of biochar composites with excellent adsorption performance by modifying and loading other materials on its surface has become a current research focus.

Similar to biochar, carbon nanotubes (CNTs), characterized by large specific surface areas and layered hollow structures are promising new adsorbents that have unique mechanical, electrical and thermal properties.[19] Previous studies have shown that carbon nanotubes have excellent binding affinity to heavy metals in aqueous solutions;[20–22] however, the application of carbon nanotubes in the removal of heavy metals is limited due to the poor solubility of these nanotubes and their tendency to aggregate into bundles. Hence, novel techniques have been developed to stabilize carbon nanotubes in order to improve

School of Life Science, Qufu Normal University, Qufu 273165, China. E-mail: yangyuewei@163.com

† The two authors contributed equally.

their capacity for application in the removal of heavy metals. Several studies have demonstrated that biochar can be used as a carrier to provide both pore space and surface sites to stabilize and distribute carbon nanotubes.[23–25] In addition, recent studies have proposed to combine biochar with nanomaterials, which can produce "engineered biochars" that would feature unique physicochemical properties and enhanced sorption capacities for the removal of heavy metals.[26] Since both biochar and nanomaterials have significant adsorption capacity, the biochar-supported nanocomposites are prospective sorbents for contaminants and can provide a new prospect for water treatment and environmental protection.

Thus, the objectives of our research are as follows: (i) to produce biochar-supported nanomaterials by an impregnation method and evaluate the potentials of nanocomposites as functional sorbents for the removal of heavy metals; (ii) to utilize Pb(II) as a model metal pollutant to examine the effect of underlying influencing factors, such as initial Pb(II) concentration, solution pH, ionic strength, utilization times of the biochar samples, reaction time and temperature, on the adsorption reaction; and (iii) to obtain insights into the mechanism of the reaction of Pb(II) with biochar-supported nanocomposites by mathematical models and characterization tools.

In the previous studies on the sorption of Pb(II) on biochar-supported CNT composites published until now, the raw materials of biochar vary, including sugar beet, animal waste residues and sweetgum biomass.[27,28] In this paper, biochar and biochar-supported nanocomposites were prepared through the slow pyrolysis of chestnut shells pre-treated with CNTs, and this study investigated the effects of different factors on the sorption of Pb(II) with biochar samples, which has not been reported so far. Moreover, biochar and biochar-supported nanocomposites were characterized by scanning electron microscopy (SEM), Fourier transform infrared spectroscopy (FTIR) and X-ray diffraction (XRD). Simultaneously, various mathematical models were used to simulate the adsorption process and contribute to the analysis of sorptive mechanism. This paper not only investigates the efficiency of the adsorption of Pb(II) on the composites, but also provides experimental basis and theoretical support for the application of biochar and its composites in treating heavy metal pollution.

2. Materials and methods

2.1 Materials

Chestnut shells were obtained from Qufu city, China, and its chemical components were phenois, organic acids, sugar, polysaccharides or glycosides, iactanes, coumarins, sterol or triterpene, tannins and flavonoids.[29,30] After being washed with distilled water, the feedstock was naturally air-dried and crushed to powder for biochar production. The carbon nanomaterials multi-walled CNTs (MWCNTs, purity > 95%, Beijing, China) with the diameters of 10–20 nm were used. Lead nitrate was purchased from Tianjin Kaitong Chemical Reagent Co., Ltd. (Tianjin, China). The chemical reagents used in this study were of analytical grade.

2.2 Preparation of the sorbents

As shown in Fig. 1, the carbon nanomaterial-biochar nanocomposites are prepared by the impregnation method. First, a nanomaterial suspension was prepared by mixing 3 g of CNT with 200 mL of deionized (DI) water, and the suspension was stirred and sonicated for 2 h in an ultrasonicator (SB-5200-DT) for the preparation of biochar-based nanocomposites. Second, 20 g chestnut shell feedstock was added to the abovementioned suspension and thoroughly dip-coated for 2 h, followed by drying in an oven at 70 °C for 48 h. Finally, the nanocomposites produced *via* slow pyrolysis for 1 h at 600 °C in a tube furnace (LTKC-6-12) under N_2 protection were obtained. In addition, feedstock without carbon nanomaterials was used to produce pristine biochar under the same pyrolysis conditions (*i.e.*, 600 °C for 1 h in an N_2 environment). The pristine biochar and biochar nanocomposites were marked as CS and CS-CNT, respectively. The biochar sorbents were washed several times with distilled water to remove potential impurities, oven-dried, and stored in containers for subsequent use. The physicochemical properties of CS and CS-CNT are presented in Table 1.

2.3 Characterization

The Brunauer–Emmett–Teller (BET) method was applied to measure the specific surface area and pore volume of the biochar samples by a surface area and porosity analyzer (Kubo, China). A Fourier transform infrared (FTIR) spectrometer (NEXUS-470, America) produced by Thermo Nicolet Corporation was used to detect surface functional groups in the wavenumber range from 4000 to 400 cm^{-1}. A scanning electron microscope (SEM; Sigma 500 VP, Carl Zeiss AG, Germany) was used to examine the morphology and structure of the samples. The crystalline structures of the biochar samples were characterized by an X-ray diffractometer (X'pert3, PANalytical, The Netherlands).

2.4 Adsorption experiments

A stock solution of Pb (500 mg L^{-1}) was prepared for subsequent dilution to expected concentrations in the batch experiments conducted to investigate the adsorption of Pb(II). Sorption experiments for each biochar sample were carried out

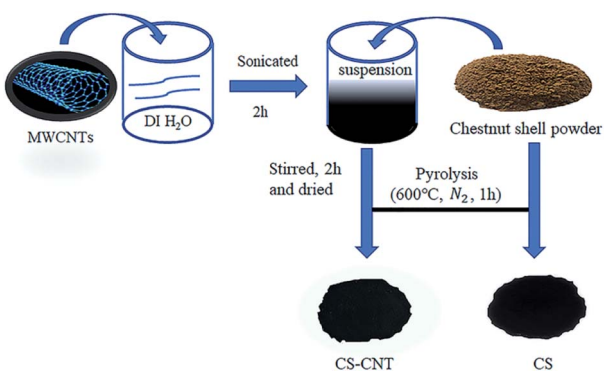

Fig. 1 Schematic for the preparation of biochar samples.

Table 1 Physicochemical properties of CS and CS-CNT

Sample	Content (%) C	H	O	N	Ash	Surface area ($m^2\ g^{-1}$)	Pore volume ($cm^3\ g^{-1}$)
CS	83.15	2.28	8.71	0.89	4.97	193.52	0.077
CS-CNT	85.89	1.63	5.53	0.64	6.31	231.60	0.09

Ash composition (wt%)

Sample	CaO	MgO	SiO_2	MnO	Al_2O_3	Fe_2O_3	Na_2O	ZnO
CS	54.99	27.37	3.77	1.69	0.99	0.42	0.02	0.25
CS-CNT	46.04	20.28	7.11	1.2	6.43	5.83	0.80	0.28

by mixing 0.03 g of the sorbent with 30 mL of Pb(II) (50 mg L^{-1}) solutions in 100 mL polyethylene plastic bottles at room temperature (22 ± 1 °C) for 24 h. These vessels were rotated at 200 rpm in a mechanical shaker (WH-782, Shanghai Jinghua Technology Instrument Co., Ltd., Shanghai, China). The initial pH of the solution was adjusted by HCl (1 or 0.1 M) and/or NaOH (1 or 0.1 M). Control experiments were performed to investigate the effects of initial Pb(II) concentration (20–200 mg L^{-1}), solution pH (2–8), ionic strength (0.1–1 mol L^{-1}), utilization times (0–4) of the biochar samples, reaction kinetics (0–48 h), and reaction isotherms (288–308 K) on the removal of Pb(II).

After the reaction, the suspensions were immediately filtered through 0.22 μm pore size nylon membrane (GE cellulose nylon membrane) filters for later analyses. All treatments were repeated three times, and the results were reported according to average values. The residual Pb(II) concentrations in the filtrates were determined using a flame atomic absorption spectrophotometer (Shimadzu AA-7000). Moreover, in this study, the Langmuir and Freundlich isotherm models were applied to describe the sorption behavior. The equations are described as follows:[31,32]

$$\frac{C_e}{q_e} = C_e\frac{1}{q_m} + \frac{1}{K_L q_m}, \text{ Langmuir}$$

$$\lg q_e = (1/n)\lg C_e + \lg K_F, \text{ Freundlich}$$

Here, C_e (mg L^{-1}) is the equilibrium concentration of the adsorbate in the solution, q_e (mg g^{-1}) is the amount of the metal adsorbed at equilibrium, q_m (mg g^{-1}) is the maximum monolayer adsorption capacity, K_L (L mg^{-1}) is the Langmuir constant, and K_F (mg g^{-1}) and n are the Freundlich constants.

Moreover, two different models were used to simulate the adsorption kinetics in this study. The equations of the two models are as follows:[33]

$$\log(q_e - q_t) = \log q_e - \frac{k_1 t}{2.303}, \text{ first-order}$$

$$\frac{t}{q_t} = \frac{1}{k_2 q_e^2} + \frac{t}{q_e}, \text{ second-order}$$

Here, q_t (mg g^{-1}) and q_e (mg g^{-1}) are the amounts of Pb(II) sorbed at time t and at equilibrium, respectively; k_1 (10^{-3}/min) and k_2 (10^{-4} g mg^{-1} min^{-1}) are the rate constants of the pseudo-first-order adsorption and pseudo-second-order adsorption, respectively.

3. Results and discussion

3.1 Characterization of biochar

3.1.1 SEM characterization and BET analysis. The SEM images of CS and CS-CNT are shown in Fig. 2. CS-CNT showed obvious distinctions in morphology and pore volume; the surfaces of CS-CNTs were porous and rough and the nanoparticles were successfully attached onto the biochar surface. The BET surface areas and pore volumes of the tested samples are presented in Table 1. The specific surface area and pore volume of CS were 193.52 $m^2\ g^{-1}$ and 0.077 $cm^3\ g^{-1}$, respectively. CS-CNT showed a significant increase in the specific surface area (231.6 $m^2\ g^{-1}$), and the pore volume values were much higher than that of CS; this reflected that the carbon nanotubes might be stabilized on the biochar surfaces and the pore networks, which could increase the surface and enlarge the pores of biochars.[34]

3.1.2 FTIR and XRD results. The spectra of the biochar samples are presented in Fig. 3(a). The FTIR spectrum of the samples can further reveal the changes in the peak positions and intensities of pristine biochar and biochar-based nanocomposites. The spectrum of CS is roughly similar to that of CS-CNT. The spectra of the biochar samples were characterized by six bands at the wavenumbers of 3433, 2927, 1622, 1430, 1081, and 667 cm^{-1}. The bands at 2927, 1622, 1430, 1081, and 667 cm^{-1} are attributed to aliphatic CH_2 deformation, –COOH and C=O group stretching, C=C stretching of the aromatic carbons in biochar samples or COO– group stretching, Si–O–Si stretching, and C–O asymmetric stretching, respectively.[35–38] As observed for all samples, the spectra of CS and CS-CNT show

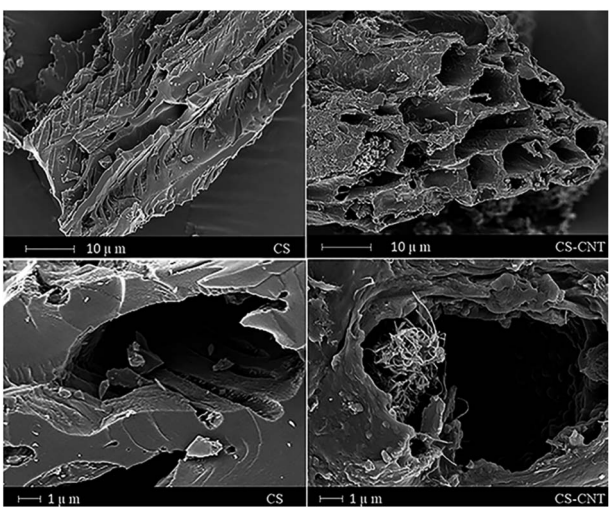

Fig. 2 SEM images of CS and CS-CNT.

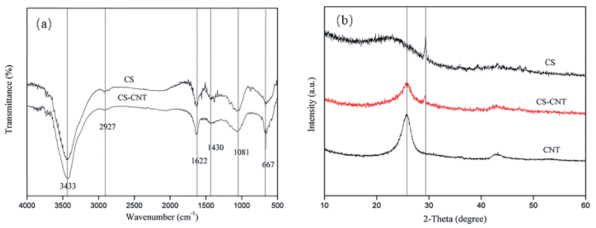

Fig. 3 FTIR spectra (a) and XRD patterns (b) of CS and CS-CNT.

a stronger band at around 3433 cm^{-1}, which is attributed to the hydroxyl (OH) stretching.[39]

The crystal structures of the biochar samples and carbon nanotubes were characterized by XRD. As seen in Fig. 3(b), there is a diffraction peak at around 25° in the XRD pattern of CS-CNT, which is due to the hexagonal graphite structure[40] and is related to the successful attachment of carbon nanotubes to biochar. The intensity of this peak decreased after the CNTs were supported by biochar, which demonstrated the presence of a turbostratic carbon structure with randomly oriented graphitic carbon layers.[41] Besides, there is a similar peak at around 28° in the XRD patterns of both the CS and CS-CNT samples; the sharp peak represents the formation of turbostratic graphite crystallites.[42,43]

3.2 Effects of different conditions on Pb(II) removal

3.2.1 Adsorption isotherms of Pb(II). Temperature is an important factor for the adsorption of heavy metals. The adsorption isotherms for the adsorption of Pb(II) on CS and CS-CNT at three different temperatures are shown in Fig. 4. It can be observed that the adsorption amount of Pb(II) on CS-CNT is significantly higher than that on CS, and the adsorption amounts of Pb(II) on both CS-CNT and CS increase with the increase in temperature; this is contrary to the observations reported in a previous study.[40] The adsorption data were described using the Langmuir and Freundlich isotherm models. The calculated adsorption isotherm parameters of Pb(II) are presented in Table 2. As observed from the isotherms

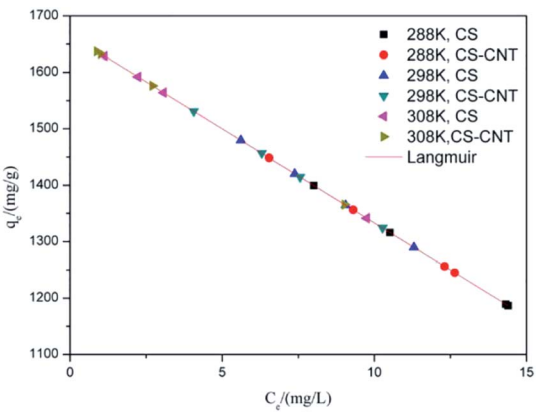

Fig. 4 Linear fitting of the adsorption isotherm by the Langmuir model.

shown in Fig. 4 and the R^2 values presented in Table 2, the Langmuir isotherm model can fit better than the Freundlich isotherm model, suggesting that the interactions between Pb(II) and the sorbents might be mainly related to mono-layer adsorption; this might be because of the homogeneous distribution of active sites on the biochar sample surfaces.[44] The maximum adsorption amount of Pb(II) on CS-CNT was significantly higher than that on CS, indicating that the presence of carbon nanomaterials enhanced the heavy metal sorption ability of biochar.

3.2.2 Adsorption kinetics of Pb(II). Herein, sorption kinetic experiments were performed to explore the reaction time and Pb(II) removal capacity of CS and CS-CNT. As shown in Fig. 5, CS-CNT can adsorb more Pb(II) than CS; the adsorption reaction is fast in the initial 15 min and then gradually slows down until the equilibrium is reached at about 12 h. Hence, the time of 12 h was chosen as the reaction time to achieve the equilibrium of the adsorption process. CS-CNT could efficiently remove Pb(II) from water, and the capacity could reach 1641 mg g^{-1}, indicating that the carbon nanomaterials on the biochar surface could serve as active sorption sites for heavy metals or enhance the surface porosity properties. Several previous studies have demonstrated that CNTs have strong sorption abilities towards various contaminants including Pb(II).[45,46]

As shown in Table 3, the Pb(II) sorption kinetics can better fit the pseudo-second-order model than the pseudo-first-order model, the R^2 values are between 0.99 and 1.0, and Q_e is nearly equal to the equilibrium value. Pb(II) ions passed into the internal surface of the biochar samples *via* liquid-film controlled diffusion. Hence, the adsorption of Pb(II) on CS and CS-CNT might be controlled by chemisorption including complexation, electrostatic attraction, and cation exchange.[47] Previous studies have demonstrated that both the biochar matrix and the carbon nanoparticles of the nanocomposites contribute to the sorption of heavy metals from aqueous solutions, which may complicate the sorption process and mechanism.[48] In addition, the functional groups on the internal and outer surfaces of the biochar samples may bind Pb(II) ions *via* "π–π dispersion interactions" and "donor–acceptor effect".[49]

3.2.3 Effects of initial concentration. The initial concentration of the solution significantly influenced the sorption of Pb(II) onto the biochar samples (Fig. 6). As observed from the sorption process of Pb(II) on the biochar samples, the sorption

Table 2 Calculated parameters of the Langmuir and Freundlich isotherms for Pb(II) adsorption

Type	Temperature (K)	Langmuir model			Freundlich model		
		q_m	k_L	R^2	K_F	$1/n$	R^2
CS	288	990.10	0.404	0.998	2554.24	−0.286	0.988
	298	1143.81	0.735	0.997	2082.24	−0.195	0.975
	308	1294.44	2.631	0.998	1690.03	−0.094	0.873
CS-CNT	288	1078.13	0.569	0.998	2244.26	−0.231	0.984
	298	1214.36	1.050	0.997	1915.11	−0.154	0.954
	308	1334.65	4.131	0.999	1643.15	−0.077	0.885

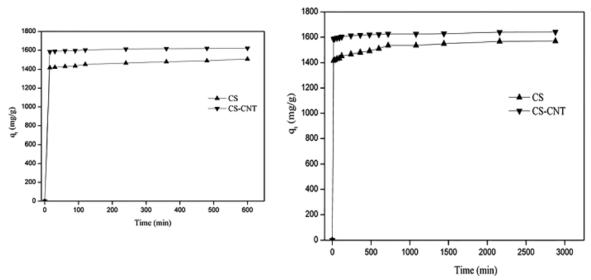

Fig. 5 Sorption kinetics of Pb(II) on CS and CS-CNT.

Table 3 Pseudo first-order and pseudo second-order kinetic parameters for Pb(II) adsorption on biochar samples

Sorbents	Equilibrium value	Pseudo first-order			Pseudo second-order		
		k_1	q_t	R^2	k_2	q_e	R^2
CS	1568.25	1.9	171.90	0.97403	0.454	1572.33	0.99989
CS-CNT	1641.26	1.3	151.05	0.95243	1.38	1640.42	0.99998

capacities of the sorbents followed the order CS-CNT > CS. The adsorption rate of Pb(II) continued to increase on increasing the concentration of the solution until the initial concentration plateaued at 50 mg L^{-1}; moreover, the maximum Pb(II) sorption capacities of CS and CS-CNT were the highest, with values greater than 1404.84 and 1450.53 mg g^{-1}, respectively. The metal sorption capacities of the biochar nanocomposites were significantly higher than that of pristine biochar, proving that the CNT particles significantly contributed to the sorption ability of the sorbents.

3.2.4 Effect of solution pH. The influence of initial solution pH on the removal efficiency of Pb(II) by the biochar samples was examined in the solution pH range of 2.0–8.0; the results are shown in Fig. 7. The solution pH exerted an influence on the sorption of heavy metals by affecting the occurrence form of heavy metal ions and the surface charge distribution of biochar. It is evident that the adsorption capacity of CS-CNT is higher

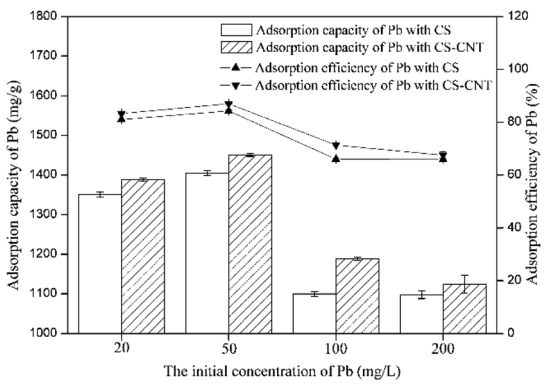

Fig. 6 Effect of initial concentration on the adsorption of Pb(II) on biochar samples.

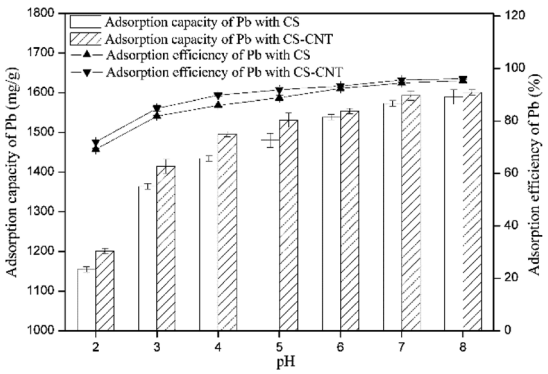

Fig. 7 Effect of pH on the adsorption of Pb(II) on biochar samples.

than that of CS when the pH varies from 5.0 to 8.0. The amount of Pb(II) adsorbed continued to increase on increasing the pH (Fig. 7). Under the condition of a low pH, the adsorption abilities of CS and CS-CNT were low; the main reason was that there were a large number of H^+ ions in the solution, which competed with the Pb(II) ions for the sorption sites.[50,51] At the same time, the amount of H^+ has an influence on the positive charge existing in the biochar samples. In this study, when pH > 5, a small amount of precipitation of the adsorbed Pb(II) occurred. It is thus reasonable to choose pH = 5 for the subsequent experiments as according to a previous study, in the pH range from 1.0 to 5.5, nearly 100% of Pb exists in the form of Pb(II),[52] whereas in some other studies, pH 6.0 has been used for Pb(II) adsorption.[53,54]

3.2.5 Effects of the ionic strength of NaCl. Ionic strength plays a significant role in the adsorption process of Pb(II). Fig. 8 shows the influence of different concentrations of NaCl on the adsorption of Pb(II) by CS and CS-CNT. The adsorption rate increased gradually with the increase in the concentration of NaCl. The reasons for this phenomenon are as follows: (1) the ability of Na^+ and Cl^- to compete with metal ions for active adsorption sites is weak and negligible; (2) with the increase in the contents of Na^+ and Cl^- in the solution, the electrostatic repulsion of Pb(II) is reduced and the adsorption of Pb(II) on the biochar samples is promoted;[55] (3) the increase in the contents of Na^+ and Cl^- may also lead to the aggregation of the adsorbent

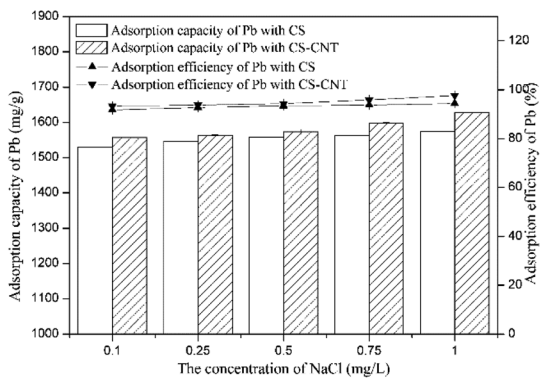

Fig. 8 Effect of ionic strength on the adsorption of Pb(II).

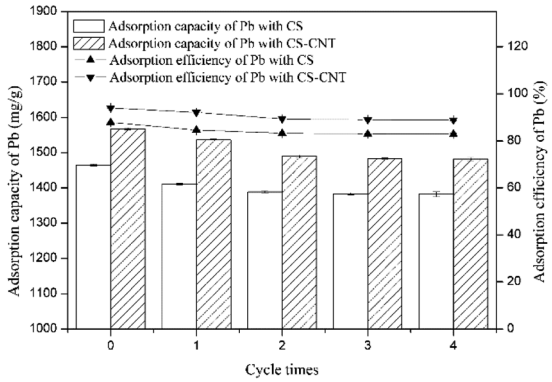

Fig. 9 Effect of the utilization times of the biochar samples on the adsorption of Pb(II).

molecules or ions, thus increasing the adsorption capacity of Pb(II).[56]

3.2.6 Effects of the utilization times of the biochar samples. In the practical applications of biochar samples, the stability and efficiency of the sorbents have been given more attention. As shown in Fig. 9, with the increase in the number of adsorption–desorption cycles, the adsorption rates of CS and CS-CNT gradually decrease. After four cycle experiments, the adsorption rates of CS and CS-CNT decreased by 4.99% and 5.17% compared with those after the first cycle of adsorption–desorption and remained at 82.92% and 88.91%, respectively. The reason for this decrease may be explained by the desorption conditions, the concentration of Pb, the sorption materials, and the concentrations of various ions in the solution.[57–59] As observed from the above-mentioned results, the sorbent reported in this study has stable adsorption performance and huge application value.

3.3 Mechanisms

The results of this study showed that the combination of carbon nanotubes with biochar could effectively improve the sorption capacity of Pb(II) in an aqueous environment. Previous studies have also demonstrated that other nanocomposites such as

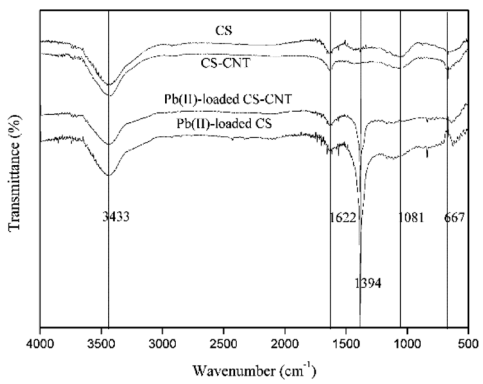

Fig. 10 FTIR spectra obtained before and after the sorption of Pb(II) on biochar samples.

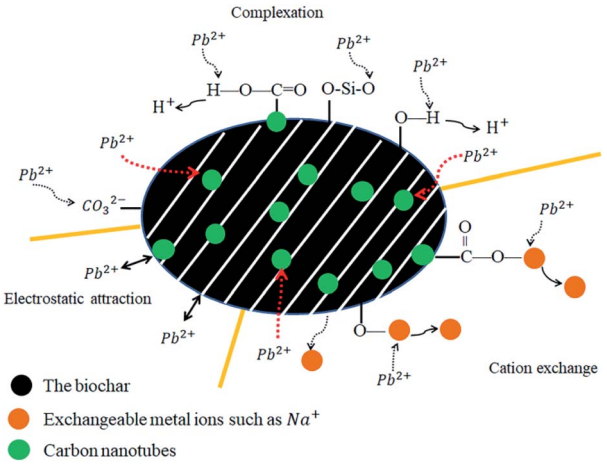

Fig. 11 Proposed mechanisms for the adsorption of Pb(II) on the biochar samples.

sand-coated carbon nanomaterials show excellent adsorption ability for heavy metals.[60,61] However, other previous studies have shown that both the biochar matrix and the carbon nanoparticles of the nanocomposites contribute to the adsorption of heavy metals, which may complicate the adsorption process and mechanism.[25]

The FTIR spectra obtained before and after the sorption of Pb(II) on CS and CS-CNT are presented in Fig. 10. After Pb(II) adsorption, the band intensity of –OH (3433 cm^{-1}) decreased and the Si–O–Si bending band (1081 cm^{-1}) almost disappeared, indicating that Pb(II) adsorbed on CS and CS-CNT through complexation with oxygen-containing functional groups. On the other hand, a new band at 1394 cm^{-1} representing the covalent Pb–CO_3 bond appeared in the spectra of CS and CS-CNT after the adsorption of Pb(II).[62] As shown in Fig. 11, the possible mechanisms of Pb(II) removal by biochar-supported nanocomposites include complexation with oxygen-containing functional groups of the sorbents, cation exchange, and electrostatic attraction with the surface of the biochar samples.[23,63,64] In addition, several studies have shown that the functional groups, such as hydroxyl groups (–COOH) and hydroxyl groups (–OH), on the biochar samples can form strong complexes with Pb(II) by the "π–π dispersion interactions" and "donor–acceptor effect".[19,49,65] Herein, the adsorption capacity of CS-CNT was higher than that of CS.

4. Conclusions

Herein, novel nanocomposites were successfully prepared *via* the direct pyrolysis of the chestnut shells pre-treated with corresponding carbon nanomaterials and used for the adsorption of Pb(II). Compared with pristine biochar, the biochar-supported nanomaterials had the highest specific surface area and porosity, which were advantageous to the adsorption process.

CS-CNT could efficiently remove Pb(II) from water under the conditions of the Pb(II) concentration of 50 mg L^{-1} and the pH value of 5. The adsorption process was fast in the initial 15 min

and reached equilibrium at about 12 h. The higher concentration of NaCl had a positive effect on Pb(II) removal; this may be due to the binding sites provided by Na^+ and Cl^-. With respect to the adsorption isotherms of Pb(II) on the biochar samples, the Langmuir model could better stimulate the sorption process. CS and CS-CNT with a high correlation coefficient value (0.997–0.9997) exhibited a mono-layer adsorption behavior. The adsorption process could be well-defined *via* the pseudo-second-order model (0.99–1.0). The adsorption of Pb(II) on CS and CS-CNT might be controlled by chemisorption including complexation, electrostatic attraction, and cation exchange. The adsorption–desorption experimental results indicate that CS-CNT has stable and excellent sorption ability for heavy metals and huge application value. These carbon nanomaterials are promising sorbents for the treatment and remediation of metal contaminants.

Conflicts of interest

There are no conflicts of interest to declare.

Acknowledgements

This research was supported by the National Natural Science Fund of China (no. 31672314 and no. 31700433).

References

1 X. Huang, H. Zhao, G. Zhang, J. Li, Y. Yang and P. Ji, *Chemosphere*, 2020, **242**, 125148.
2 A. Naeem, M. T. Saddique, S. Mustafa, Y. Kim and B. Dilara, *J. Hazard. Mater.*, 2009, **168**, 364–368.
3 Y. Zhou, X. Liu, L. Tang, F. Zhang, G. Zeng, X. Peng, L. Luo, Y. Deng, Y. Pang and J. Zhang, *J. Hazard. Mater.*, 2017, **333**, 80–87.
4 Y. Zhou, F. Zhang, L. Tang, J. Zhang, G. Zeng, L. Luo, Y. Liu, P. Wang, B. Peng and X. Liu, *Sci. Rep.*, 2017, **7**, 43831.
5 F. Fu and Q. Wang, *J. Environ. Manage.*, 2011, **92**, 407–418.
6 M. I. Inyang, B. Gao, Y. Ying, Y. Xue, A. Zimmerman, A. Mosa, P. Pullammanappallil, S. O. Yong and X. Cao, *Crit. Rev. Environ. Sci. Technol.*, 2016, **46**, 406–433.
7 Z. Yu, Z. Chang, Z. Zheng, H. Liang, X. Li, Z. Yang, M. Chi and G. Zeng, *Appl. Surf. Sci.*, 2017, **403**, 413–425.
8 C. H. Cheng, J. Lehmann, J. E. Thies, S. D. Burton and M. H. Engelhard, *Org. Geochem.*, 2006, **37**, 1477–1488.
9 A. Demirbas, *J. Anal. Appl. Pyrolysis*, 2004, **72**, 243–248.
10 L. Beesley and M. Marmiroli, *Environ. Pollut.*, 2011, **159**, 474–480.
11 H. M. S. K. Herath, M. Camps-Arbestain and M. Hedley, *Geoderma*, 2013, **209–210**, 188–197.
12 M. Ahmad, A. U. Rajapaksha, J. E. Lim, Z. Ming, N. Bolan, D. Mohan, M. Vithanage, S. L. Sang and S. O. Yong, *Chemosphere*, 2014, **99**, 19–33.
13 Z. Liu, X. Chen, J. Yan, Q. Li, J. Zhang and Q. Huang, *Catena*, 2014, **123**, 45–51.
14 T. Wang, C. E. Stewart, C. Sun, Y. Wang and J. Zheng, *Catena*, 2018, **162**, 29–39.
15 J. Shi, H. Han and C. Xu, *Sci. Total Environ.*, 2019, **697**, 134052.
16 K. Wang, Y. Sun, J. Tang, J. He and H. Sun, *Chemosphere*, 2020, **241**, 125044.
17 T. R. Bridle and D. Pritchard, *Water Sci. Technol.*, 2004, **50**, 169–175.
18 E. B. Ledesma, N. D. Marsh, A. K. Sandrowitz and M. J. Wornat, *Energy Fuels*, 2002, **16**, 1331–1336.
19 G. P. Rao, C. Lu and F. Su, *Sep. Purif. Technol.*, 2007, **58**, 224–231.
20 L. Ouni, A. Ramazani and S. T. Fardood, *Front. Chem. Sci. Eng.*, 2019, **13**, 274–295.
21 A. A. Farghali, H. A. A. Tawab, S. A. A. Moaty and R. Khaled, *J. Nanostruct. Chem.*, 2017, **7**, 101–111.
22 S. A. Kosa, G. Al-Zhrani and M. A. Salam, *Chem. Eng. J.*, 2012, **181–182**, 159–168.
23 M. Inyang, B. Gao, A. Zimmerman, M. Zhang and H. Chen, *Chem. Eng. J.*, 2014, **236**, 39–46.
24 M. Zhang, B. Gao, Y. Yao, Y. Xue and M. Inyang, *Sci. Total Environ.*, 2012, **435–436**, 567–572.
25 M. Inyang, B. Gao, A. Zimmerman, Y. Zhou and X. Cao, *Environ. Sci. Pollut. Res.*, 2015, **22**, 1868–1876.
26 N. Jiang, Y. Xu, Y. Dai, W. Luo and L. Dai, *J. Hazard. Mater.*, 2012, **215–216**, 17–24.
27 M. I. Inyang, MPhil thesis, Dissertations & Theses - Gradworks, 2013.
28 T. Liu, B. Gao, J. Fang, B. Wang and W. X. Cao, *RSC Adv.*, 2016, **6**(29), 24314–24319.
29 G. Vázquez, J. González-Alvarez, J. Santos, M. S. Freire and G. Antorrena, *Ind. Crops Prod.*, 2009, **29**, 364–370.
30 Z. De-yi, G. Wen-hai, H. Cheng-wen, G. X. feng and L. Chun-long, *Shaanxi Forest Science and Technology*, 2003, **2**, 1–3.
31 N. Velmurugan, G. Hwang, M. Sathishkumar, T. K. Choi, K.-J. Lee, B.-T. Oh and Y.-S. Lee, *J. Environ. Sci.*, 2010, **22**, 1049–1056.
32 G. Ghanizadeh, G. Asgari, A. M. S. Mohammade and M. T. Ghaneian, *Fresenius Environ. Bull.*, 2012, **21**, 1296–1302.
33 X. Wang, L. Chen, S. Xia, J. Zhao, J.-M. Chovelon and N. J. Renault, *Miner. Eng.*, 2006, **19**, 968–971.
34 T. Liu, B. Gao, J. Fang, W. Bing and X. Cao, *RSC Adv.*, 2016, **6**, 24314–24319.
35 H. Yuan, T. Lu, Y. Wang, H. Huang and Y. Chen, *J. Anal. Appl. Pyrolysis*, 2014, **110**, 277–284.
36 Q. Wang, B. Wang, X. Lee, J. Lehmann and B. Gao, *Sci. Total Environ.*, 2018, **634**, 188–194.
37 H. Omar R, *Environ. Sci. Technol.*, 2011, **45**, 5550.
38 P. S. Kumar, S. Ramalingam, V. Sathyaselvabala, S. D. Kirupha, A. Murugesan and S. Sivanesan, *Korean J. Chem. Eng.*, 2012, **29**, 756–768.
39 S. V. Novais, M. D. O. Zenero, M. S. C. Barreto, C. R. Montes and C. E. P. Cerri, *Sci. Total Environ.*, 2018, **633**, 825–835.
40 X. W. Zengsheng Zhang, Y. Wang, S. Xia, L. Chen, Y. Zhang and J. Zhao, *J. Environ. Sci.*, 2013, **25**, 1044–1053.
41 L. C. A. Oliveira, R. V. R. A. Rios, J. D. Fabris, V. Garg, K. Sapag and R. M. Lago, *Carbon*, 2002, **40**, 2177–2183.

42 A. A. Al-Joubori and C. Suryanarayana, *J. Mater. Sci.*, 2018, **53**, 7877–7890.

43 S. Shi, J. Yang, S. Liang, M. Li, Q. Gan, K. Xiao and J. Hu, *Sci. Total Environ.*, 2018, **628–629**, 499–508.

44 W. Du, J. Sun, Y. Zan, Z. Zhang, J. Ji, M. Dou and F. Wang, *RSC Adv.*, 2017, **7**, 46629–46635.

45 J. Xu, Z. Cao, Y. Zhang, Z. Yuan, Z. Lou, X. Xu and X. Wang, *Chemosphere*, 2018, **195**, 351–364.

46 R. Kumar, M. A. Khan and N. Haq, *Crit. Rev. Environ. Sci. Technol.*, 2014, **44**, 1000–1035.

47 R. Shi, Y. Li, J. Yin and S. Yang, *Chin. J. Environ. Eng.*, 2014, **8**, 3428–3432.

48 I. Mandu, G. Bin, Z. Andrew, Z. Yanmei and C. Xinde, *Environ. Sci. Pollut. Res.*, 2014, **22**, 1868–1876.

49 M. Vithanage, S. S. Mayakaduwa, I. Herath, S. O. Yong and D. Mohan, *Chemosphere*, 2016, **150**, 781–789.

50 R. Sitko, E. Turek, B. Zawisza, E. Malicka, E. Talik, J. Heimann, A. Gagor, B. Feist and R. Wrzalik, *Dalton Trans.*, 2013, **42**, 5682.

51 Y. Xiao, Y. Xue, F. Gao and A. Mosa, *J. Taiwan Inst. Chem. Eng.*, 2017, **80**, 114–121.

52 D. Kołodyńska, R. Wnętrzak, J. J. Leahy, M. H. B. Hayes, W. Kwapiński and Z. Hubicki, *Chem. Eng. J.*, 2012, **197**, 295–305.

53 Z. Ying, C. Bo, L. Zhao, L. Sun, G. Yan, J. Li, Y. Fan, Z. Ying, C. Bo and L. Zhao, *Appl. Surf. Sci.*, 2017, 427.

54 X. Liu, D. Lai and Y. Wang, *J. Hazard. Mater.*, 2019, **361**, 37–48.

55 M. Campinas and M. J. Rosa, *J. Colloid Interface Sci.*, 2006, **299**, 520–529.

56 Y. S. Al-Degs, M. I. El-Barghouthi, A. H. El-Sheikh and G. M. Walker, *Dyes Pigm.*, 2008, **77**, 16–23.

57 H. J. Cui, M. K. Wang, M. L. Fu and E. Ci, *J. Soils Sediments*, 2011, **11**, 1135.

58 B. Wang, J. Lehmann, K. Hanley, R. Hestrin and A. Enders, *Chemosphere*, 2015, **138**, 120–126.

59 A. Bogusz, P. Oleszczuk and R. Dobrowolski, *Environ. Geochem. Health*, 2019, **41**, 1663–1674.

60 V. Datsyuk, M. Kalyva, K. Papagelis, J. Parthenios, D. Tasis, A. Siokou, I. Kallitsis and C. Galiotis, *Carbon*, 2008, **46**, 833–840.

61 W. Gao, M. Majumder, L. B. Alemany, T. N. Narayanan, M. A. Ibarra, B. K. Pradhan and P. M. Ajayan, *ACS Appl. Mater. Interfaces*, 2011, **3**, 1821–1826.

62 T. Zhang, X. Zhu, L. Shi, J. Li and Y. Li, *Bioresour. Technol.*, 2017, **235**, 185–192.

63 V. K. Gupta, S. Agarwal and T. A. Saleh, *J. Hazard. Mater.*, 2011, **185**, 17–23.

64 V. K. Gupta, I. Tyagi, S. Agarwal, O. Moradi and A. Garshasbi, *Crit. Rev. Environ. Sci. Technol.*, 2016, **46**, 93–118.

65 G. Zhao, J. Li, X. Ren, C. Chen and X. Wang, *Environ. Sci. Technol.*, 2011, **45**, 10454–10462.